Two-photon absorption and second harmonic generation of 1*S* para- and orthoexcitons in Cu_2O coupled by a magnetic field

A. Farenbruch,[1] D. Fröhlich,[1] D. R. Yakovlev,[1,2] and M. Bayer[1,2]
[1]*Experimentelle Physik 2, Technische Universität Dortmund, D-44221 Dortmund, Germany*
[2]*Ioffe Institute, Russian Academy of Sciences, 194021 St. Petersburg, Russia*

(Received 30 May 2020; revised 4 August 2020; accepted 20 August 2020; published 10 September 2020)

We report on two-photon absorption (TPA) and second harmonic generation (SHG) spectroscopy of para- and orthoexcitons in Cu_2O subject to a strong magnetic field up to 10 T. The magnetic field splits the orthoexciton into its three quasispin components $M = 0, \pm 1$ and activates the symmetry and spin forbidden paraexciton by an admixture from the $M = 0$ component of the orthoexciton. For the excitation of the paraexciton we suggest an alternative mechanism of TPA without an external perturbation. It involves instead of the electric dipole-electric dipole the electric quadrupole-magnetic dipole excitation process. By application of group theory we derive for both mechanisms of TPA and SHG polarization selection rules for each of the four resonances (one para- and three orthoexcitons) and present experimental results for different crystalline orientations which agree perfectly with the derivations from group theory. High spectral resolution of the used SHG technique allows us to refine the exchange splitting between the para- and orthoexciton of $\varepsilon = 12.120$ meV and the g values of the upmost valence band $g_v = -0.72 \pm 0.03$ and the lowest conduction band $g_c = 2.38 \pm 0.08$.

DOI: 10.1103/PhysRevB.102.115203

I. INTRODUCTION

The 1*S* paraexciton of the yellow exciton series of Cu_2O has gained a lot of interest mainly as a candidate for the observation of Bose-Einstein condensation (BEC). For a recent review on these attempts we refer to Ref. [1]. The paraexciton is the lowest energy exciton in Cu_2O. From the upmost valence band (Γ_7^+ symmetry) and the lowest conduction band (Γ_6^+ symmetry) one derives the threefold orthoexciton (Γ_5^+ symmetry) and the single paraexciton (Γ_2^+ symmetry). The paraexciton is a pure spin triplet state 12.1 meV [2] below the orthoexciton. The small exciton radius of the 1*S* exciton of 0.7 nm [3] leads to the rather large exchange splitting of 12.1 meV. In linear optical spectroscopy the paraexciton can only be excited if an external perturbation like stress [4] or magnetic field [2,5] is applied, which leads to an admixture of the orthoexciton to the pure triplet paraexciton and thus to a nonvanishing oscillator strength. In a high quality natural crystal a very narrow paraexciton resonance of 80 neV was measured [2].

In Ref. [6] details of two-photon magnetoabsorption of para- and orthoexcitons are derived. The low sensitivity of the two-photon absorption (TPA) experiments, however, did not allow us to detect paraexcitons. Resonant two-photon absorption of the 1*S* paraexciton in a potential trap is reported in Refs. [7–9]. Here the paraexciton gets allowed by strain-induced admixture of the 1*S* green orthoexciton [4].

TPA for odd parity excitons without external perturbation can be achieved by replacing one of the electric dipole operators in the TPA process by a magnetic dipole operator as was shown in alkali halides in Ref. [10] and for GaAs in Ref. [11]. In Cu_2O, however, we are dealing with even parity excitons. For the direct TPA excitation of the paraexciton (Γ_2^+ symmetry) the other odd parity electric dipole operator (Γ_4^- symmetry) has to be replaced by the even parity electric quadrupole operator (Γ_5^+ symmetry). There are thus two mechanisms to excite the paraexciton in Cu_2O: (i) by electric dipole-electric dipole (DD) excitation of the orthoexciton admixture either by a magnetic field or strain or (ii) by direct two-photon electric quadrupole-magnetic dipole (QMD) excitation. The latter excitation is expected to be rather weak, since two higher order processes are needed to excite the even parity paraexciton.

For both mechanisms (i) and (ii) we will derive the detailed polarization dependencies by merely group theoretical techniques. In Ref. [12] we did not take into account the degeneracy of the excited states (e.g., threefold excitons of Γ_5^+ symmetry) for the derivation of polarization selection rules, which was sufficient for the higher excited exciton states ($n \geqslant 3$) to distinguish between the different processes considered (magneto-Stark and Zeeman effect). For the 1*S* excitons, however, one has to take into account the threefold degeneracy of the orthoexciton and the single paraexciton, which are coupled by a magnetic field and split into three separate orthoexciton components ($M = \pm 1, M = 0$) and the 12.1 meV lower paraexciton. As shown in detail in Ref. [12] we will only use the tables of Koster *et al.* [13] to derive for any crystalline orientation the polarization dependence for the different excitation channels of TPA and second harmonic generation (SHG) of paraexcitons.

The paper is organized as follows: In Sec. II details of the experiments are explained. In Sec. III we derive the magnetic field dependence of the 1*S* para- and orthoexcitons and present experimental results. From the spectra we extract the

 ©2020 American Physical Society

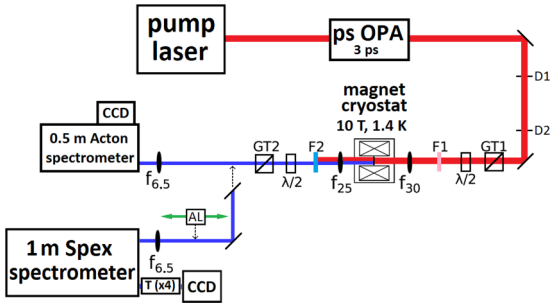

FIG. 1. Setup for SHG spectroscopy: AL, alignment laser; CCD, charge-coupled device; D, diaphragm; F, color filter; f_{xx}, lens with xx-cm focal length; GT, Glan Thompson linear polarizer; $\lambda/2$, half-wave plate; OPA, optical parametric amplifier; T(×4), telescope with a magnification factor of four. The double side alignment laser (AL) in front of the 1 m Spex spectrometer is useful for aligning the SHG beam into the Spex spectrometer.

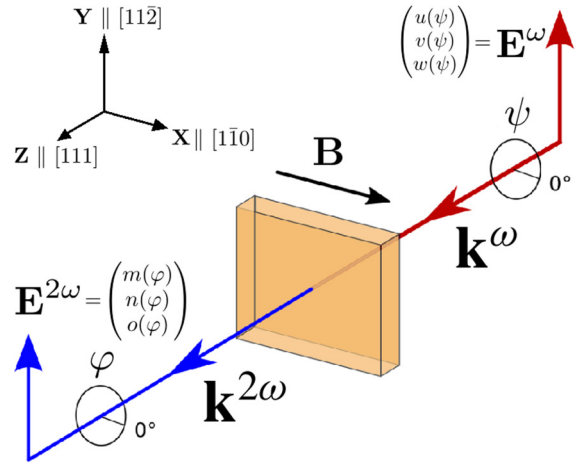

FIG. 2. Example of an experimental geometry in Voigt configuration: $\mathbf{k} \parallel \mathbf{Z} \parallel [111]$, $\mathbf{X} \parallel \mathbf{B} \parallel [1\bar{1}0]$, and $\mathbf{Y} \parallel [11\bar{2}]$.

exchange splitting, g values, and the magnetic field dependent oscillator strength of the paraexciton. In Sec. IV A we derive the TPA and SHG polarization dependencies for the three orthoexciton components and the paraexciton. In Sec. IV B experimental results of TPA and SHG polarization dependencies are shown and compared to simulations derived in Sec. IV A. In Sec. V we present conclusions and an outlook. In Appendix A we show a full diagonalization of the magnetic field interaction and band structure effects [14], which is relevant for the low field regime ($B < 0.1$ T). In Appendix B we show two-dimensional (2D) polarization diagrams for selected crystalline orientations of direction $\mathbf{k}$ of the exciting laser beam. We distinguish between Voigt (magnetic field $\mathbf{B} \perp \mathbf{k}$) and Faraday configuration ($\mathbf{B} \parallel \mathbf{k}$).

II. EXPERIMENT

The experimental setup is shown in Fig. 1. For more details we refer to Ref. [12]. For the spectra of the magnetic field dependence of para- and orthoexcitons we used the 1 m Spex spectrometer in first order (resolution 20 μeV [12]). The polarization dependencies were recorded with the 0.5 m Acton spectrometer, since the signals are by a factor 4 larger than in the 1 m Spex setup and the lower resolution (80 μeV) is for the polarization dependence of no relevance.

The samples are cut from a natural Cu_2O crystal. For the TPA experiments we use a 5.1 mm thick sample with the orientation $\mathbf{k} \parallel \mathbf{Z} \parallel [11\bar{2}]$, $\mathbf{B} \parallel \mathbf{X} \parallel [111]$, and $\mathbf{Y} \parallel [1\bar{1}0]$. For the SHG experiments by DD excitation we use a 30 μm thick sample with the orientation $\mathbf{k} \parallel \mathbf{Z} \parallel [111]$, $\mathbf{B} \parallel \mathbf{X} \parallel [1\bar{1}0]$, and $\mathbf{Y} \parallel [11\bar{2}]$. This orientation is shown in Fig. 2. For the SHG experiments by QMD excitation we use a 50 μm thick sample with the orientation $\mathbf{k} \parallel \mathbf{Z} \parallel [001]$, $\mathbf{B} \parallel \mathbf{X} \parallel [1\bar{1}0]$, and $\mathbf{Y} \parallel [110]$.

For all measurements the samples were mounted strain-free and cooled to $T = 1.4$ K in superfluid helium. For the polarization dependent experiments the polarizer angle ψ and the analyzer angle φ can be tuned independently. For the 1D polarization diagrams the polarization angle was tuned in steps of 5° and for the 2D polarization diagram both polarization angles (ψ, φ) were tuned in steps of 10°. The magnetic field dependent exciton intensities are measured in steps of 0.5 T up to 10 T.

In order to separate the excitation of the paraexciton from the much more efficient excitation of the orthoexciton we used the picosecond optical parametric amplifier (OPA). It emits pulses with a duration of 3.3 ps at a repetition rate of 30 kHz. The laser beam with an average power of 60 mW is focused onto the sample to a spot with a diameter of 100 μm, which results in an intensity of 7.7 GW cm^{-2}. The spectral width of the picosecond pulse is determined by a measurement of the second harmonic in a BBO (beta Barium Borate) crystal placed in the excitation beam behind the cryostat. The width of 1.1 meV is much less than the separation of the para- and orthoexciton of 12.1 meV, thus leading to a sufficient suppression of a direct excitation of orthoexcitons. The spectra are obtained by setting the central photon energy of the laser at half of the exciton energy (2.0206 eV for the paraexciton and 2.0328 eV for the orthoexcitons).

As a demonstration of the high resolution and high signal-to-noise ratio we present in Fig. 3 spectra of the 1S orthoexcitons and the paraexciton, which were taken with the

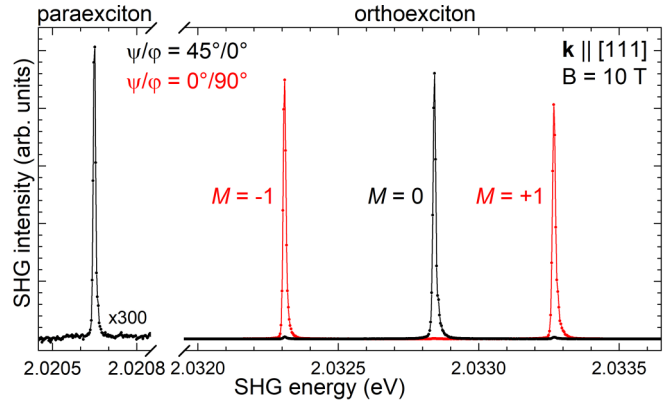

FIG. 3. SHG spectrum of the orthoexciton ($M = 0$, $M = \pm 1$) and the paraexciton at $B = 10$ T in Voigt geometry. The 30 μm thick sample is oriented with $\mathbf{k} \parallel [111]$, $\mathbf{B} \parallel [1\bar{1}0]$ and $\mathbf{E}^{\omega,2\omega}(90°) \parallel [11\bar{2}]$ (Fig. 2). The spectrum is measured with a resolution of 10 μeV.

1 m Spex spectrometer in second order (resolution 10 μeV) in a magnetic field of 10 T. The polarization settings indicated in the graph are derived for arbitrary crystalline and magnetic field orientations in Sec. IV A.

In Sec. III we derive for the ratio of the ortho- to paraexciton oscillator strength $f_o/f_p(10\,\mathrm{T}) \approx 177$. For the ratio of the SHG signals in Fig. 3 we get a ratio of ≈300. In our derivation of the polarization dependencies we did not take phase matching [15] into account. For para- and orthoexcitons we expect perfect phase matching on the upper polariton branches [16,17]. For the orthoexciton, however, the expected higher reabsorption of the orthoexciton might be the reason for this discrepancy.

III. MAGNETO-OPTICAL SPECTROSCOPY OF PARA- AND ORTHOEXCITONS

In this section we first derive the theory of the 1S para- and the 1S orthoexciton. From spectra taken in a magnetic field up to 10 T we extract the relevant parameters (as exchange splitting and g values) and compare them to literature values from linear optical experiments. We diagonalize the 4×4 Zeeman matrix and neglect the impact of the valence band structure as derived in Ref. [14], since it turns out that the $\mathbf{k}^2$ dependent perturbation, which was first interpreted as being due to a $\mathbf{k}^2$ exchange term [18], has a measurable effect only in the low-field regime ($B < 0.2$ T). The full diagonalization including band structure effects is given in Appendix A. The expected splitting and field dependence is beyond our spectral resolution. From a fit of the field dependence we will derive the relevant parameters (exchange splitting ε, g values of valence and conduction band g_v and g_c) and magnetic field dependent oscillator strength $f_p(B)$ of the paraexciton.

Neglecting $\mathbf{k}^2$ effects due to the band structure we start with the 4×4 matrix in the $M = 0, \pm 1$ basis for the orthoexciton and the paraexciton, which interacts with the $M = 0$ component of the orthoexciton. We get for the Zeeman Hamiltonian [6]

$$H_{\mathrm{Zeeman}}(a,b,B) = \begin{pmatrix} -\varepsilon & -iaB & 0 & 0 \\ iaB & 0 & 0 & 0 \\ 0 & 0 & -bB & 0 \\ 0 & 0 & 0 & bB \end{pmatrix}, \quad (1)$$

where ε is the exchange splitting, $a = \mu_B(g_c - g_v)/2$ is the ortho/para mixing parameter, $b = \mu_B(g_c + g_v)/2$ is the splitting parameter of the orthoexciton [6], and μ_B is the Bohr magneton.

The diagonalization of the Zeeman matrix [Eq. (1)] leads to the eigenvalues for the field dependence of the orthoexciton components ($E_{o,M}$ with $M = 0, \pm 1$) and the paraexciton E_p:

$$E_p = \frac{1}{2}(-\varepsilon - \sqrt{\varepsilon^2 + 4a^2B^2}) \approx -\varepsilon - \frac{a^2B^2}{\varepsilon}, \quad (2)$$

$$E_{o,0} = \frac{1}{2}(-\varepsilon + \sqrt{\varepsilon^2 + 4a^2B^2}) \approx \frac{a^2B^2}{\varepsilon}, \quad (3)$$

$$E_{o,\pm 1} = \pm bB. \quad (4)$$

The magnetic field dependent admixture of the orthoexciton to the paraexciton is derived from the eigenfunction $\psi_p(B) = \alpha(B)|\Gamma_2^+\rangle + \beta(B)|\Gamma_{5,o}^+\rangle$. The admixture parameters of the eigenvector are given by

$$\alpha(B) \approx \frac{1}{\sqrt{1 - \left(\frac{aB}{\varepsilon}\right)^2}} \approx 1, \quad (5)$$

$$\beta(B) \approx \frac{iaB}{\varepsilon\sqrt{1 - \left(\frac{aB}{\varepsilon}\right)^2}} \approx \frac{iaB}{\varepsilon}. \quad (6)$$

Since SHG of the paraexciton gets allowed by its admixture to the orthoexciton the field-dependent oscillator strength for the paraexciton f_p [2] is given by

$$f_p(B) = |\beta(B)|^2 f_o, \quad (7)$$

where f_o is the oscillator strength of the orthoexciton.

In Fig. 4 we present the magnetic field dependence of the SHG energies of the three components of the orthoexciton and the paraexciton. The spectral positions are gained by a fit of the SHG lines by Gaussians. For the fit of the magnetic field dependent spectral positions of the exciton components, we use Eq. (2) for the paraexciton, Eq. (3) for the $M = 0$, and Eq. (4) for the $M = \pm 1$ orthoexciton components. It is noted that the fits of the orthoexciton components do not intersect at the same energy at 0 T. This is explained by the derivation in

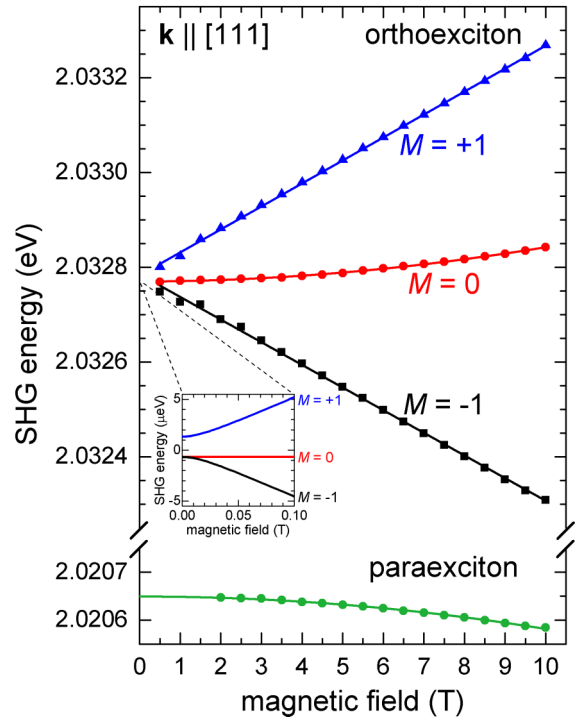

FIG. 4. Magnetic field dependence of the orthoexciton ($M = 0$, $M = \pm 1$) and the paraexciton. The dots represent measured data and the lines represent the fits. The $M = \pm 1$ components of the orthoexciton show a linear shift in energy. The paraexciton and the $M = 0$ component of the orthoexciton show a quadratic shift. The inset diagram shows the additional splitting due to the band structure, which is relevant for low magnetic fields. This is discussed in more detail in Appendix A. The 30 μm thick Cu_2O sample is oriented with $\mathbf{k} \parallel [111]$, $\mathbf{B} \parallel [1\bar{1}0]$, and $\mathbf{E}^{\omega,2\omega}(90°) \parallel [11\bar{2}]$. The spectra are measured with the 1 m Spex spectrometer in first order with a resolution of 20 μeV (Sec. II).

TABLE I. Comparison of ε and g values with literature data.

Source	ε (meV)	g_c	g_v	$\lvert g_c + g_v \rvert$	$\lvert g_c - g_v \rvert$
this paper	12.120	2.38	−0.72	1.66	3.1
[5]	12	2.68	−1.02	1.66	3.70
[6]		3.17	−1.53	1.64	4.70
[20]	12.117				3.26
[21]				1.7	

Appendix A and shown in the inset of Fig. 4. Strain induced splitting of the components as discussed in Ref. [19] could also be of relevance. The parameters of the fits are:

$$a = 91 \pm 3 \ \frac{}{\mu\text{eV}}\text{T}, \tag{8}$$

$$|g_c - g_v| = 3.1 \pm 0.1, \tag{9}$$

$$b = 48.1 \pm 0.3 \ \frac{}{\mu\text{eV}}\text{T}, \tag{10}$$

$$|g_c + g_v| = 1.66 \pm 0.01, \tag{11}$$

$$\varepsilon = 12.120 \text{ meV}, \tag{12}$$

$$f_p(B) = (5.6 \pm 0.4) \times 10^{-5} B^2 f_o. \tag{13}$$

For the g values we get

$$g_c = 2.38 \pm 0.08, \tag{14}$$

$$g_v = -0.72 \pm 0.03. \tag{15}$$

A comparison of the parameters of different sources is presented in Table I. Compared to the literature values, our fits lead to slightly different parameters for ε and the g values, which might be due to the fact that the SHG resonances are expected to be slightly shifted as compared to the one-photon absorption data of Refs. [2,18] due to the polariton dispersion.

The field dependent oscillator strength $f_p(B)$ agrees well with the value derived from high resolution data (Ref. [2], $f_p(B) = 5.8 \times 10^{-5} B^2 f_o$). According to the theory the ratio of oscillator strengths is $f_o/f_p(10\,\text{T}) \approx 177$.

IV. POLARIZATION DEPENDENCIES OF PARA- AND ORTHOEXCITONS

In Sec. IV A we derive the polarization dependencies of para- and orthoexcitons by a group theory analysis for DD as well as QMD excited TPA and SHG. In Sec. IV B we present experimental data of the polarization dependencies and compare them to the calculations.

A. Theory of polarization dependencies

In this subsection we present the theory of two-photon absorption (TPA) and second-harmonic generation of the 1S para- and orthoexcitons of Cu_2O. The paraexciton as a spin triplet is forbidden to all orders for electric dipole transitions [7]. By application of an external perturbation as, e.g., strain [4] or a magnetic field [2,5] the paraexciton gets allowed by its admixture to the orthoexciton. The paraexciton can thus be observed in TPA and also in SHG.

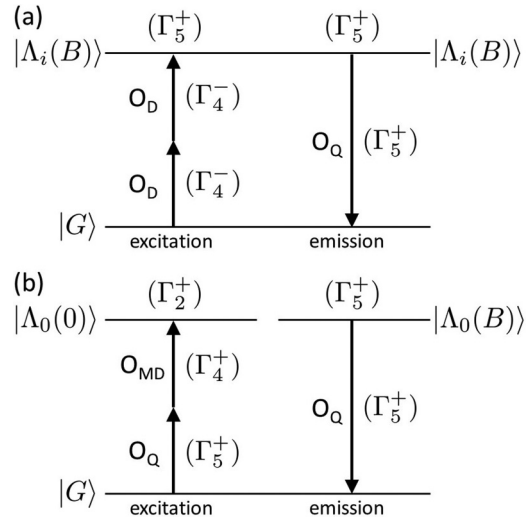

FIG. 5. Schematics of the SHG processes. (a) Excitation of eigenvectors $\Lambda_i(B)$ of para- and orthoexcitons by Γ_5^+ DD excitation and Γ_5^+ electric quadrupole emission. (b) Excitation of eigenvector $\Lambda_0(0)$ by Γ_2^+ QMD excitation and Γ_5^+ electric quadrupole emission from $\Lambda_0(B)$.

As outlined in the introduction there is a new mechanism of direct excitation of the paraexciton without external perturbation: Instead of a magnetic field (Zeeman operator of Γ_4^+) the coupling between the singlet-triplet mixed orthostates and the pure triplet paraexciton is already achieved in the two-photon excitation process by replacing the two odd-parity electric dipole operators (Γ_4^- symmetry) by two even parity operators (electric quadrupole operator of Γ_5^+ symmetry and magnetic dipole operator of Γ_4^+ symmetry). Obviously the magnetic dipole operator replaces the Zeeman operator in the mixing process.

TPA of paraexcitons is thus allowed without application of a static magnetic field. Experimentally, however, TPA by QMD excitation could not be detected, since excitation spectroscopy experiments (e.g., by detection through phonon side bands of the paraexciton) were not successful up to now, since impurity emission in our natural crystals does not allow us to resolve emission from the paraexciton. SHG, however, needs the Zeeman operator to couple the directly excited paraexciton to the Γ_5^+ orthoexciton, which then allows electric quadrupole emission. This new QMD excitation mechanism can only be detected in Voigt configuration in a fourfold crystalline direction (e.g., $\mathbf{k} \parallel [001]$ and $\mathbf{B} \parallel [010]$ or [110]). The SHG process by DD and by QMD excitation are sketched in Fig. 5.

As outlined in the introduction we have to take into account the threefold degeneracy of the orthoexciton, which is coupled to the single paraexciton by a magnetic field. We therefore start with the diagonalization of the 4×4 matrix taking into account the exchange splitting ε and Zeeman effect. For the derivation of the polarization dependence for arbitrary crystalline and magnetic field orientation we have to start with the 4×4 matrix in the basis of the single paraexciton (Γ_2^+ symmetry) and the three orthoexciton components (Γ_{5yz}^+, Γ_{5zx}^+,

Γ^+_{5xy}). We thus get for the Zeeman matrix [22]:

$$M_B(a,b,\mathbf{B}) = \begin{pmatrix} -\varepsilon & iaB_x & iaB_y & iaB_z \\ -iaB_x & 0 & -ibB_z & ibB_y \\ -iaB_y & ibB_z & 0 & -ibB_x \\ -iaB_z & -ibB_y & ibB_x & 0 \end{pmatrix}. \quad (16)$$

For the derivation of the polarization dependence of TPA and SHG of the four resonances (three orthoexcitons and one paraexciton) we need the four eigenvectors $|\Lambda_i(B)\rangle$ ($i = 0..3$), where each eigenvector has four components. From the matrix [Eq. (1)] it is obvious that there is an admixture of the paraexciton only to the $M = 0$ orthoexciton. As will be discussed in Appendix A, in general this is not valid, if $\mathbf{k}^2$ effects are taken into account [14].

The polarization dependence of TPA is derived in terms of second order [23] and for SHG in terms of third order perturbation theory. In the second order excitation process we have to distinguish between DD excitation (only Γ^+_5 contribution) and QMD excitation (only Γ^+_2 contribution), whereas for the additional first order emission process in SHG we apply for both cases the electric quadrupole operator (only Γ^+_5 contribution). We proceed as in Ref. [12] with the difference that the magnetic-field dependence (magnetic field orientation and strength) is taken care of in the eigenvectors $|\Lambda_i(B)\rangle$. For the nomenclature of the relevant physical quantities we follow closely Ref. [12]. The orientations are sketched in Fig. 2.

As in Ref. [12], we start our analysis with the rotation matrix:

$$M_{\mathrm{rot}}(\mathbf{k},\psi) = \begin{pmatrix} k_1^2(1-\cos\psi)+\cos\psi & k_1k_2(1-\cos\psi)-k_3\sin\psi & k_1k_3(1-\cos\psi)+k_2\sin\psi \\ k_2k_1(1-\cos\psi)+k_3\sin\psi & k_2^2(1-\cos\psi)+\cos\psi & k_2k_3(1-\cos\psi)-k_1\sin\psi \\ k_3k_1(1-\cos\psi)-k_2\sin\psi & k_3k_2(1-\cos\psi)+k_1\sin\psi & k_3^2(1-\cos\psi)+\cos\psi \end{pmatrix}, \quad (17)$$

where $\mathbf{k} = (k_1, k_2, k_3)^{\mathrm{T}}$ is the normalized wave vector of light. By multiplying the horizontal crystal direction $\mathbf{X}$ with the rotation matrix, we get the polarization vectors $\mathbf{E}^{\omega}(\psi)$ and $\mathbf{E}^{2\omega}(\varphi)$ for the in- and outgoing light:

$$\mathbf{E}^{\omega}(\psi) = (u(\psi), v(\psi), w(\psi))^{\mathrm{T}} = M_{\mathrm{rot}}(\mathbf{k},\psi)\cdot\mathbf{X}, \quad (18)$$

$$\mathbf{E}^{2\omega}(\varphi) = (m(\varphi), n(\varphi), o(\varphi))^{\mathrm{T}} = M_{\mathrm{rot}}(\mathbf{k},\varphi)\cdot\mathbf{X}. \quad (19)$$

We now define the relevant operators for the different excitation and emission processes. The TPA operator for Γ^+_5 excitation [23] is given by

$$O_{\mathrm{DD}}(\psi) = \sqrt{2}\begin{pmatrix} 0 \\ v(\psi)w(\psi) \\ u(\psi)w(\psi) \\ u(\psi)v(\psi) \end{pmatrix}, \quad (20)$$

the electric quadrupole operator for the outgoing photon is given by

$$O_{\mathrm{Q}}(\mathbf{k},\varphi) = \frac{1}{\sqrt{2}}\begin{pmatrix} 0 \\ k_2o(\varphi)+k_3n(\varphi) \\ k_1o(\varphi)+k_3m(\varphi) \\ k_1n(\varphi)+k_2m(\varphi) \end{pmatrix}, \quad (21)$$

and the magnetic dipole operator is given by

$$O_{\mathrm{MD}}(\mathbf{k},\psi) = \frac{1}{\sqrt{2}}\begin{pmatrix} 0 \\ k_2w(\psi)-k_3v(\psi) \\ -k_1w(\psi)+k_3u(\psi) \\ k_1v(\psi)-k_2u(\psi) \end{pmatrix}. \quad (22)$$

Since the eigenvectors $\Lambda_i(B)$ have four components and the polarization dependencies are derived from scalar products of the $\Lambda_i(B)$ and the operators, the operators are extended to four components. The first component in each operator vanishes, since none of them leads to an excitation of the paraexciton.

We derive the TPA polarization dependence from second order perturbation theory [23]. From the necessary condition of a nonvanishing excitation matrix element we derive the polarization dependencies for TPA via DD excitation processes:

$$\langle\Lambda_i(B)|O_{\mathrm{DD}}(\mathbf{k},\psi)|G\rangle \neq 0. \quad (23)$$

Since $|G\rangle$ as the ground state transforms as $|\Gamma^+_1\rangle$, the Γ^+_1 contribution of the direct product and thus the scalar product of $\Lambda_i(B)$ and $O_{\mathrm{DD}}(\mathbf{k},\psi)$ leads to

$$I^{2\omega}_{\mathrm{TPA,DD},i}(\mathbf{k},\psi,B) \propto |\Lambda_i(B)\cdot O_{\mathrm{DD}}(\mathbf{k},\psi)|^2. \quad (24)$$

For each of the four eigenvectors ($i = 0$: paraexciton, $i = 1$: $M = 0$ orthoexciton and $i = 2, 3$: $M = \pm1$ orthoexcitons) we derive a polarization dependence, where the paraexciton and the $M = 0$ orthoexciton should exhibit the same polarization dependence, as seen from the 4×4 matrix [Eq. (1)]. It turns out that TPA of paraexcitons can be excited in Voigt configuration for $\mathbf{k} \parallel [110]$, $[111]$, and $[112]$, but not for $\mathbf{k} \parallel [001]$. As shown in Ref. [12] TPA is detected by excitation spectroscopy from exciton phonon side bands or impurities. Since the paraexciton eigenvector depends linearly on the magnetic field strength, a B^2 field dependence is expected for the TPA intensity of the paraexciton. As expected $I^{2\omega}_{\mathrm{TPA,DD},0}(\mathbf{k},\psi,B)$ vanishes for $B = 0$, since the paraexciton eigenvector $\Lambda_0(0) = (1,0,0,0)^T$ is orthogonal to $O_{\mathrm{DD}}(\mathbf{k},\psi)$ [Eq. (20)].

From Eq. (21) [rewritten for the polarization vector of the incoming photon $E^{\omega}(\psi)$] and Eq. (22) we derive from the Koster tables the two-photon operator for QMD excitation of the Γ^+_2 paraexciton:

$$O_{\mathrm{QMD}}(\mathbf{k},\psi) = O_{\mathrm{Q}}(\mathbf{k},\psi)\cdot O_{\mathrm{MD}}(\mathbf{k},\psi)/\sqrt{3}. \quad (25)$$

For the QMD excitation we get again the necessary condition for a nonvanishing matrix element:

$$\langle\Lambda_0(0)|O_{\mathrm{QMD}}(\mathbf{k},\psi)|G\rangle \neq 0. \quad (26)$$

Since $O_{\mathrm{QMD}}(\mathbf{k}, \psi)$ is a scalar and $\Lambda_0(0)$ is a unit vector this leads to TPA of the paraexciton via QMD excitation to:

$$I^{2\omega}_{\mathrm{TPA,QMD},0}(\mathbf{k}, \psi, B) \propto |O_{\mathrm{QMD}}(\mathbf{k}, \psi)|^2. \quad (27)$$

TPA of the paraexciton is thus for QMD excitation independent of B. It turns out that the scalar $O_{\mathrm{QMD}}(\mathbf{k}, \psi)$ vanishes for $\mathbf{k} \parallel [110]$ and $[111]$ but does not vanish for $\mathbf{k} \parallel [112]$ and $[001]$. One thus expects for these crystalline orientations a paraexciton resonance at $B = 0$, which might be detected by excitation spectroscopy via the Γ_5^+ phonon side band of the paraexciton.

For the derivation of the SHG polarization dependence we have to apply third order perturbation theory, since the para- and orthoexciton excited by two-photon processes [Eqs. (24) and (27)] have to be coupled to the ground state by the electric quadrupole operator [Eq. (21)]. For the DD excitation we get the condition:

$$\langle G|O_{\mathrm{Q}}(\mathbf{k}, \varphi)|\Lambda_i(B)\rangle\langle\Lambda_i(B)|O_{\mathrm{DD}}(\mathbf{k}, \psi)|G\rangle \neq 0. \quad (28)$$

The polarization dependence for the outgoing photon is given by the scalar product of $\Lambda_i(B)$ and $O_{\mathrm{Q}}(\mathbf{k}, \varphi)$. The polarization dependence of SHG is thus for DD excitation given by:

$$I^{2\omega}_{\mathrm{SHG,DD},\,i}(\mathbf{k}, \psi, \varphi, B) \propto |[\Lambda_i(B) \cdot O_{\mathrm{Q}}(\mathbf{k}, \varphi)][\Lambda_i(B) \cdot O_{\mathrm{DD}}(\mathbf{k}, \psi)]|^2. \quad (29)$$

It turns out that SHG of paraexcitons can be DD excited in the following configurations of $\mathbf{k}/\mathbf{B}$: $[111]/[11\bar{2}]$, $[111]/[\bar{1}10]$, $[11\bar{2}]/[\bar{1}10]$, but not in $[11\bar{2}]/[111]$, $[1\bar{1}0]/[001]$, $[1\bar{1}0]/[110]$. Since TPA for $\mathbf{k} \parallel [001]$ is not allowed in Voigt configuration there is no SHG possible. An overview is given for Voigt configuration in Fig. 11 and for Faraday configuration in Fig. 12 in Appendix A. Since there are two field dependent eigenvectors involved in the SHG signal, a B^4 dependence is expected for the SHG intensity of the paraexciton.

For the SHG by QMD excitation of the paraexciton we get:

$$I^{2\omega}_{\mathrm{SHG,QMD},0}(\mathbf{k}, \psi, \varphi, B) \propto |[\Lambda_0(B) \cdot O_{\mathrm{Q}}(\mathbf{k}, \varphi)][O_{\mathrm{QMD}}(\mathbf{k}, \psi)]|^2. \quad (30)$$

In this case only the magnetic field dependence of the eigenvector for the outgoing photon is relevant. A B^2 field dependence is thus expected for the paraexciton. It has to be noted that the mechanism of QMD excitation can easily be extended to excitation of orthoexcitons by coupling the electric quadrupole operator [Eq. (21) rewritten for the polarization vector of the incoming photon $\mathbf{E}^{\omega}(\psi)$] and the magnetic dipole operator [Eq. (22)] to Γ_5^+ (orthoexcitons) by use of the Koster tables.

We do not consider these processes, since for the Γ_5^+ orthoexcitons the signals are expected to be too weak because of the higher order QMD mechanism excitation process as compared to DD excitation. As pointed out, the excitation of the paraexciton by the higher order is only detected in the crystalline orientation ($\mathbf{k} \parallel [001]$), where SHG by DD excitation is forbidden. Examples of TPA and SHG polarization dependencies as well as magnetic field dependencies will be presented with the experimental results in Sec. IV B.

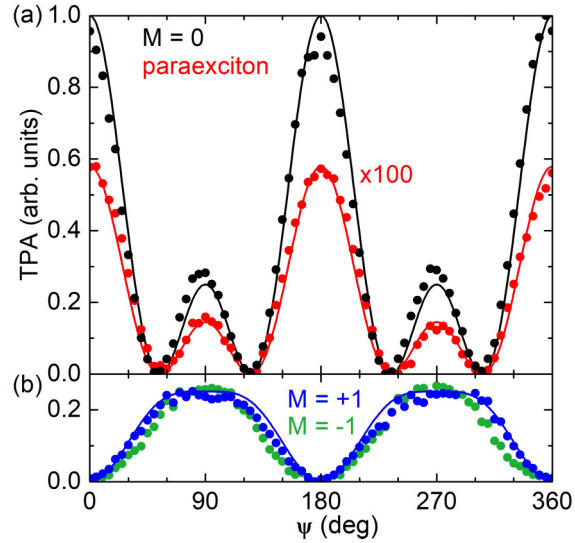

FIG. 6. TPA polarization dependence of para- and orthoexcitons as a function of ingoing polarization angle ψ at $B = 10\,\mathrm{T}$. Experimental results (dots) of TPA are monitored by the emission from the Γ_3^- phonon side bands 13.5 meV below the corresponding para- or orthoexciton. Simulations are solid lines as calculated from Eq. (24). (a) The para- and $M = 0$ orthoexciton as well as (b) the $M = \pm 1$ orthoexcitons show the same polarization dependence. The TPA signal of the paraexciton is multiplied by a factor of 100. The experimental configuration is $\mathbf{k} \parallel \mathbf{Z} \parallel [11\bar{2}]$, $\mathbf{B} \parallel \mathbf{X} \parallel [111]$, and $\mathbf{Y} \parallel [1\bar{1}0]$.

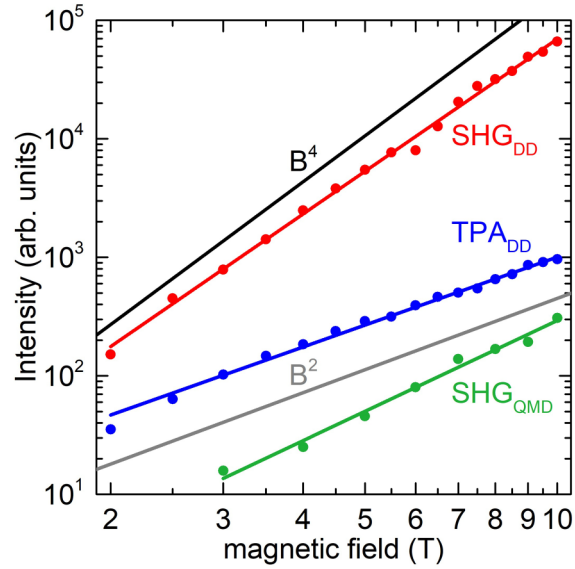

FIG. 7. Experimental results (dots) of magnetic field dependent intensities and fits (solid lines): TPA by DD excitation (blue), fit leads to $B^{1.91\pm0.04}$, B^2 (gray line) expected from Eq. (24). SHG by DD excitation (red), fit leads to $B^{3.71\pm0.08}$, B^4 (black line) expected from Eq. (29)]. SHG by QMD excitation (green), fit leads to $B^{2.5\pm0.2}$, B^2 (gray line) expected from Eq. (30). For a clear presentation of the magnetic field dependent mechanisms appropriate scaling factors are chosen for their intensities.

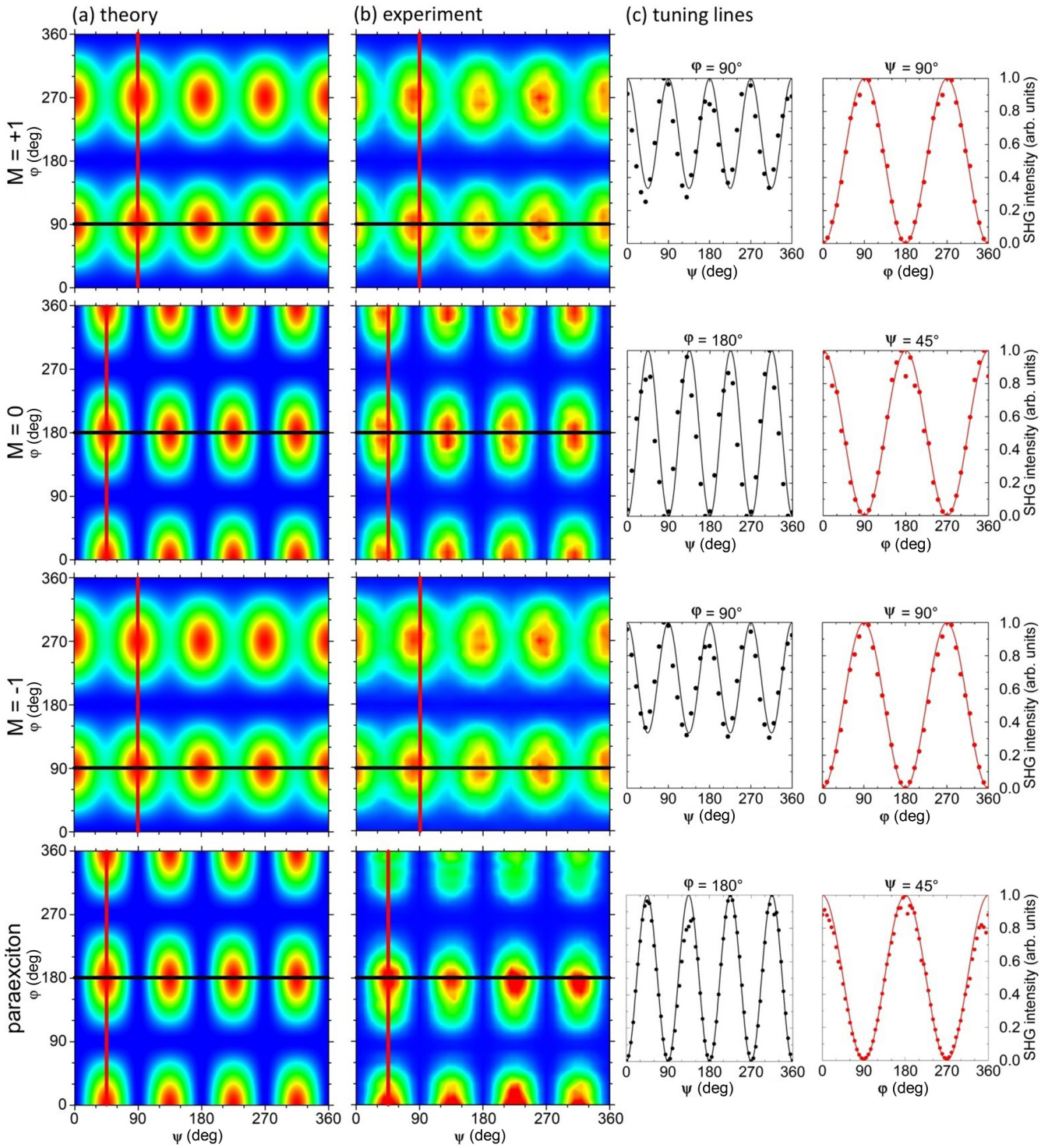

FIG. 8. (a) Theory and (b) experiment of 2D polarization dependent intensity of SHG by DD excitation [according to Fig. 5(a) and Eq. (29)] of 1S orthoexcitons at $B = 7$ T and of the paraexciton at 2.0206 eV and $B = 10$ T. Blue, light blue, yellow, green, and red indicate 0%, 25%, 50%, 75%, and 100% of maximum SHG intensity, respectively. In (c) we show the ψ- and φ-tuning lines of the experimental data (dots) and simulation (solid line) corresponding to the black and red lines in (a) and (b). As expected, the paraexciton exhibits the same polarization dependence as the $M = 0$ component of the orthoexciton. The experimental configuration is $\mathbf{k} \parallel \mathbf{Z} \parallel [111]$, $\mathbf{B} \parallel \mathbf{X} \parallel [1\bar{1}0]$, and $\mathbf{Y} \parallel [11\bar{2}]$, as shown in Fig. 2.

B. Experimental results of polarization dependencies

In this section we present our experimental results together with simulations with reference to the TPA and SHG polarization dependencies derived in Sec. IV A. In the DD mechanism [Fig. 5(a)] the paraexciton (Γ_2^+ symmetry) is excited by its magnetic field induced admixture to the $M = 0$

component of the orthoexciton (Γ_5^+ symmetry). As an example for a TPA polarization dependence we have chosen in Fig. 6 the configuration $\mathbf{k} \parallel [11\bar{2}]$ and $\mathbf{B} \parallel [111]$ (Voigt configuration). We show the TPA dependence as a function of ψ, where $\psi = 0^\circ$ corresponds for this configuration to the [111] crystalline direction and thus $\psi = 90^\circ$ to $[1\bar{1}0]$. As expected the paraexciton and the $M = 0$ orthoexciton exhibit the same polarization dependence and also the $M = +1$ and $M = -1$ components. The $M = 0$ orthoexciton simulation is normalized to 1. The other components are scaled accordingly. Experiments are scaled to simulations. There is good agreement of the polarization dependencies between experiment (dots) and simulations (solid lines) according to Eq. (24).

In Fig. 7 we present experimental results of B-dependent intensities for different excitation mechanisms. Deviations of the fits from the expected magnetic field dependence (B^2 and B^4) might be caused by slight misalignment or strain. In the case of QMD excitation the alignment of the $\mathbf{k}^\omega$ is very critical, because a slight misalignment might lead to signals via the much stronger DD excitation mechanism, which exhibits a B^4 dependence and thus might be the reason for the measured $B^{2.5}$ instead of the expected B^2 dependence.

In Fig. 8 we present experimental results and simulations [according to Eq. (29)] of the 2D and 1D polarization dependent SHG intensities of the para- and orthoexcitons for the orientation $\mathbf{k} \parallel [111]$ and $\mathbf{B} \parallel [1\bar{1}0]$. The $M = \pm 1$ resonances exhibit the same polarization dependence with a fourfold ψ dependence on a constant SHG of 1/3 of the maximum value and a twofold φ dependence [Fig. 8(c)]. The $M = 0$ component of the orthoexciton exhibits the same polarization dependence as the paraexciton. The experimental 1D diagram along selected tuning lines exhibit a fourfold pattern with a 90° period for a tuning of the laser polarization ψ with SHG polarization φ fixed to 180° [Fig. 8(c)]. The SHG polarization dependence as a function of φ ($\psi = 45^\circ$) exhibits the expected twofold pattern, which is determined by the contribution of the electric quadrupole operator [Eq. (21)] in Eq. (29). From a comparison of Fig. 8(a) (simulation) and Fig. 8(b) of the paraexciton SHG one can notice approximately 25% weaker maxima at $\varphi = 360^\circ$ in the experimental 2D diagram. This might be explained by an intensity drift of the exciting picosecond laser during the long scan time of four hours. In Fig. 7 the expected B^4 dependence of the paraexciton SHG by DD excitation according to Eq. (29) is well confirmed.

As addressed already in the introduction the QMD excitation leads to a direct population of the pure spin triplet paraexciton, since no admixture to the singlet/triplet mixed orthoexciton by an external magnetic field is necessary. It turns out that TPA by QMD excitation [Eq. (27) and Fig. 5(b)] is allowed for $\mathbf{k} \parallel [001]$, where TPA by DD excitation [Eq. (24) and Fig. 5(a)] is forbidden. Because of two second order processes in the two-photon QMD excitation the oscillator strength is expected to be much smaller than for the DD excitation.

By careful alignment of $\mathbf{k} \parallel [001]$, where TPA and SHG are forbidden for DD excitation, we succeeded to detect SHG for QMD excitation. TPA by this excitation mechanism was not detected, because it could not be distinguished from luminescence from impurities in our natural samples.

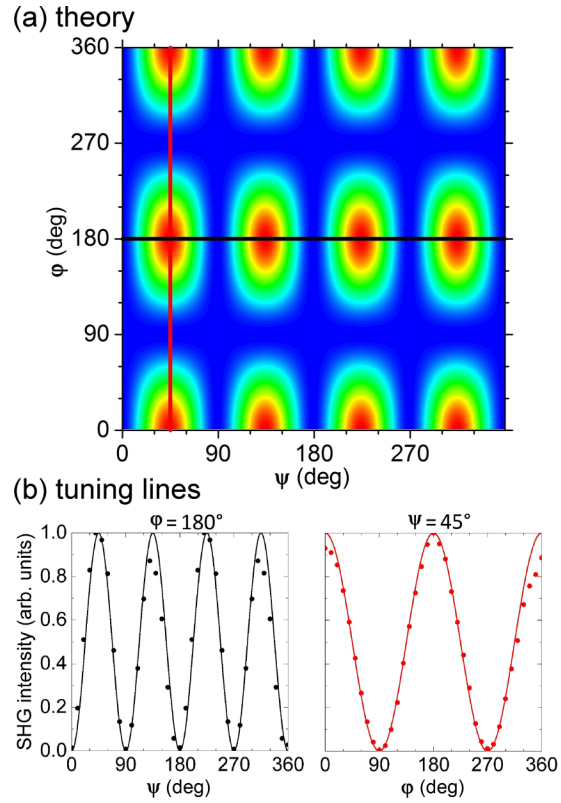

FIG. 9. SHG polarization dependence for paraexciton by QMD excitation. (a) 2D diagram derived from Eq. (30) [Fig. 5(b)] with tuning lines for experiments (dots) shown in (b) together with the corresponding simulations (lines). The experimental configuration is $\mathbf{k} \parallel \mathbf{Z} \parallel [001]$, $\mathbf{B} \parallel \mathbf{X} \parallel [110]$, and $\mathbf{Y} \parallel [\bar{1}10]$.

In Fig. 9 we present the simulation of SHG [2D diagram (a) derived from Eq. (30)] and 1D diagrams (b) for the tuning lines marked in (a). Because of the weak signals (about 1/200) compared to those by DD excitation (e.g., Fig. 8), we did not succeed to measure the full 2D diagram. The theoretical 1D diagram for TPA [Eq. (27)] exhibits the same ψ dependence as SHG for fixed $\varphi = 180^\circ$.

The QMD mechanism might be interpreted as nonresonant dynamical Zeeman effect [24,25], where the 1S orthoexciton is coupled to the paraexciton by the magnetic component of the photon field. If the coupling to light is treated nonperturbatively, this would lead to a Hamiltonian equivalent to Eq. (1). The off-diagonal elements of the frequency-dependent magnetic dipole operator couple the ortho- to the paraexciton. This effect is equivalent to the optical Stark effect in Cu_2O [26]. In this experiment the 1S exciton is resonantly coupled to the 2P exciton by a tunable CO_2 laser. For a resonant Zeeman effect in our case we would need a light source at 12.1 meV (photon wavelength of 102 μm).

V. CONCLUSIONS AND OUTLOOK

In this paper we have presented theoretical and experimental results for the nonlinear magneto-optical properties of the 1S para- and orthoexciton of the lowest exciton series (yellow series) in Cu_2O. The paraexciton is of special interest, since it is the lowest resonance and a pure spin-triplet state and thus

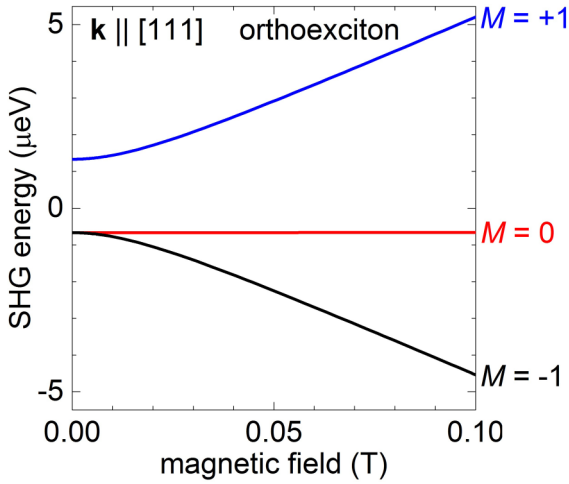

FIG. 10. Magnetic field dependent energies of the orthoexciton components ($M = 0, M = \pm 1$) resulting from the diagonalization of the sum of the Zeeman- and band structure matrix given in Eq. (A1), plotted in the magnetic field range of 0 to 0.1 T. The calculation is done for the orientation **k** ∥ [111] and **B** ∥ [1$\bar{1}$0]. The zero SHG energy marks the energy position of the unperturbed orthoexciton.

forbidden for excitation in linear optics. The magnetic-field dependent SHG spectra of the 1*S* para- ($M = 0$ admixture to paraexciton) and orthoexcitons ($M = 0$, $M = \pm 1$ components) are measured in magnetic fields up to 10 T. From the diagonalization of the relevant 4×4 matrix, electron and hole *g* values and the exchange splitting are derived, which agree well with data from linear optical experiments. Compared to a previous publication [12], we first diagonalize the 4×4 matrix of the coupled para- and orthoexcitons and then derive polarization selection rules for TPA and SHG for each of the four components. For the group theoretical treatment, the eigenvectors as well as the photon interaction operators have to be taken into account. We suggest a QMD mechanism of two-photon excitation, which is applied to the paraexciton. Contrary to the classical DD excitation the QMD mechanism allows a two-photon excitation of paraexcitons without external perturbation. For SHG one needs a perturbation like a magnetic field leading to a B^2 dependence for the QMD mechanism as compared to a B^4 dependence for DD excitation.

Detailed polarization dependencies are derived for arbitrary crystalline and magnetic field orientations. Despite the fact that for the QMD mechanism two higher order processes (QMD instead of DD excitation) are required and thus much weaker signals are expected, we succeeded to detect SHG by the QMD mechanism by the choice of a special configuration (**k** ∥ [001]) where SHG by DD excitation is forbidden. We report experimental results for SHG of both mechanisms in

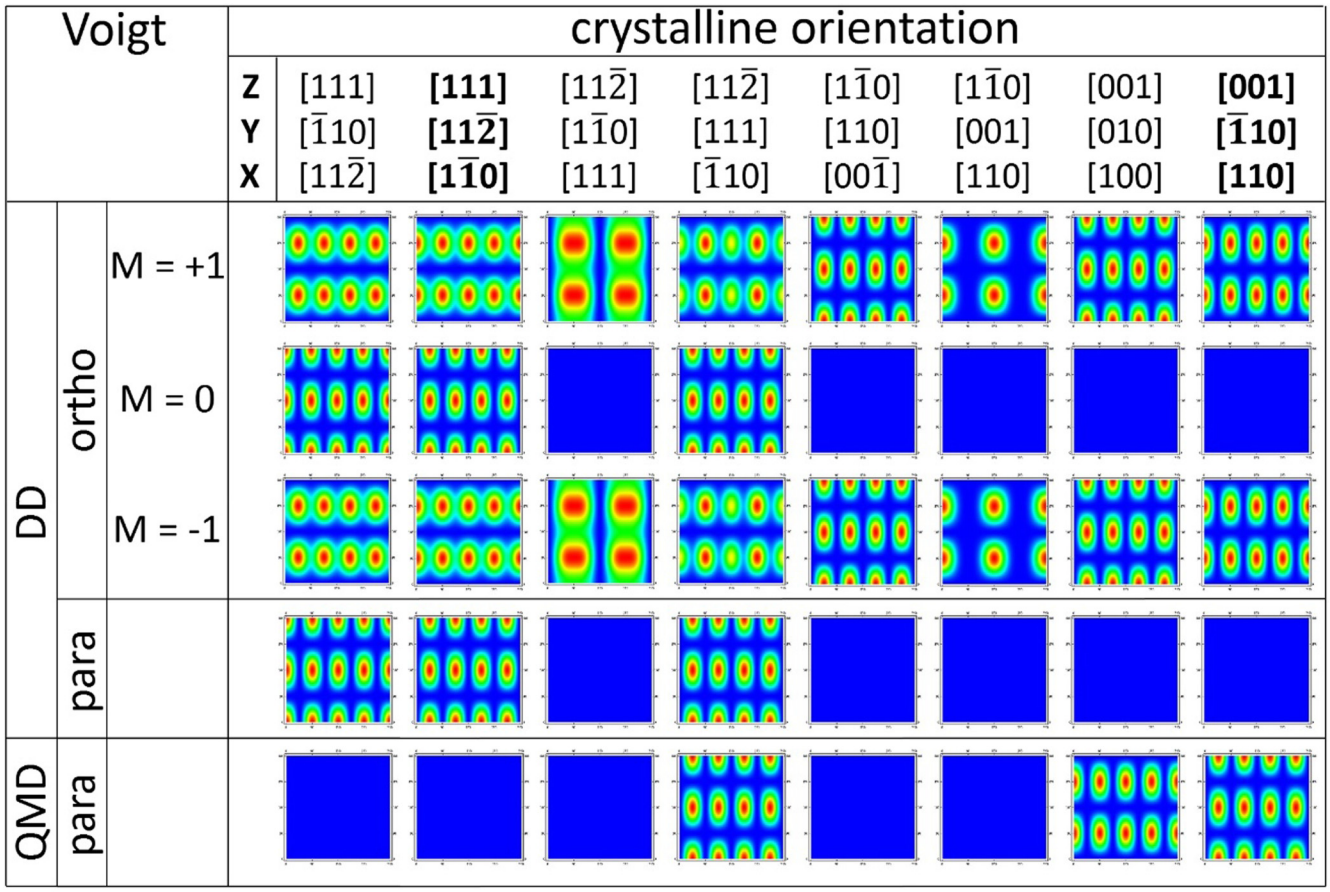

FIG. 11. 2D polarization diagrams of SHG of the four 1*S* components in Voigt configuration (**k** ∥ **Z** and **B** ∥ **X**) for selected crystalline orientations. Experimental results are taken in the configuration (**Z** ∥ [111], **Y** ∥ [11$\bar{2}$], and **X** ∥ [1$\bar{1}$0] for DD excitation and **Z** ∥ [001], **Y** ∥ [$\bar{1}$10], and **X** ∥ [110] for QMD excitation) as marked in bold.

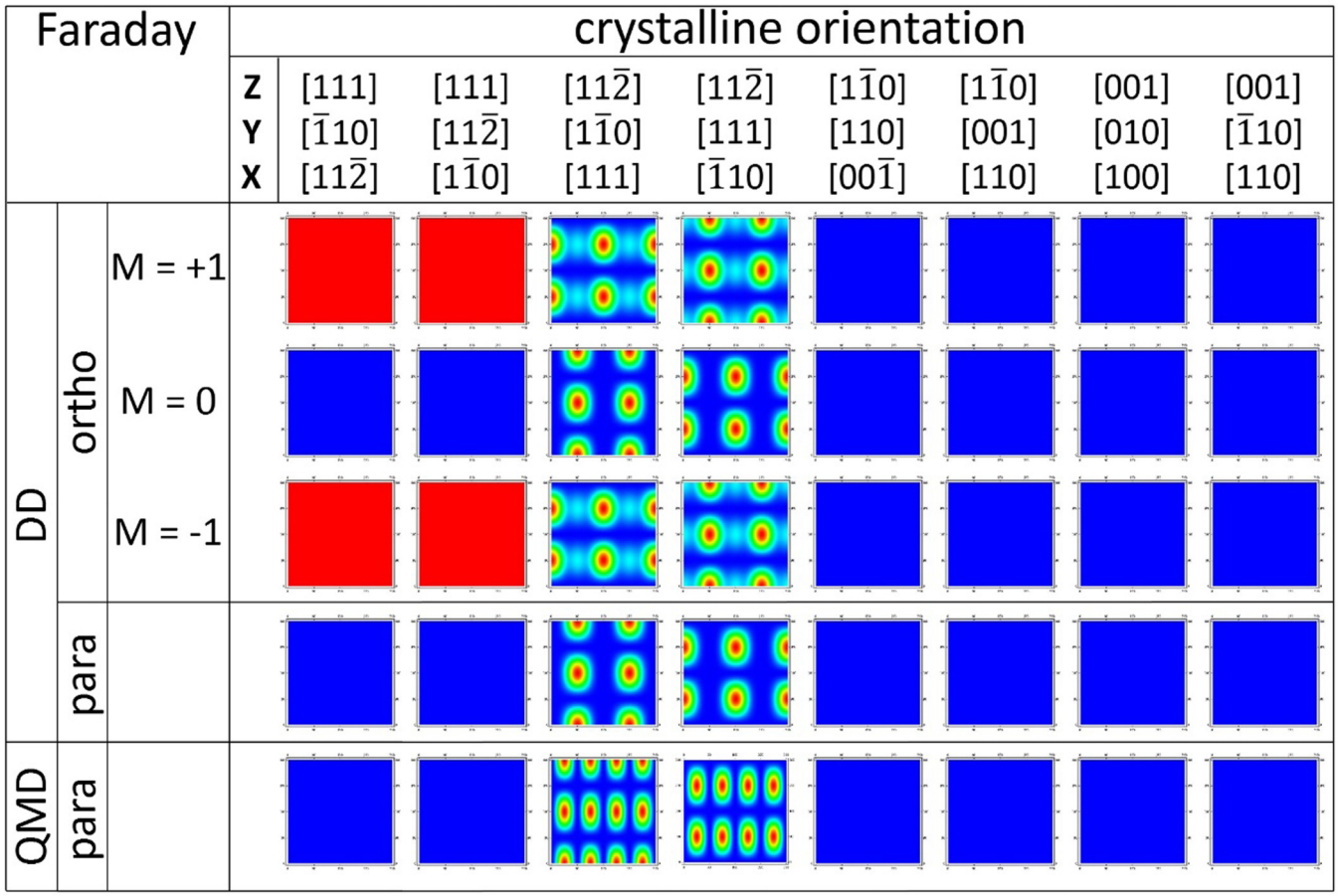

FIG. 12. 2D polarization diagrams of SHG of the four 1*S* components in Faraday configuration (**k** ∥ **B** ∥ **Z**) for selected crystalline orientations. The red diagrams show a constant nonzero SHG intensity of the $M = \pm 1$ components for all polarization angles.

Voigt configuration which in all cases confirm the derivations of Sec. IV A. TPA by the QMD mechanism, however, was not seen up to now because we did not succeed to distinguish the expected weak Γ_5^+ phonon emission of the paraexciton from impurity luminescence in our natural crystals. Thermal treatment of the samples might help to overcome this problem.

As an outlook we propose further nonlinear optical experiments to detect BEC [1]. Two-photon excitation leads to polaritons of low group velocity ($\approx 10^{-5}$ of speed of light) [17], thus increasing the density as compared to the outside photon flux. Excitation at half of the paraexciton energy might also be advantageous as compared to resonant excitation in a trap, since high intensity resonant excitation leads to nonlinear excitation of continuum states, thus causing larger heating of the sample as compared to resonant two-photon excitation. It is certainly of interest to compare two-photon excitation with one-photon excitation in a trap, where hints of a BEC were claimed [27].

ACKNOWLEDGMENTS

We appreciate helpful discussions with M. M. Glazov, M. A. Semina, and E. L. Ivchenko. We acknowledge the financial support by the Deutsche Forschungsgemeinschaft through the International Collaborative Research Center TRR160 (Project A8 and C8) and the Collaborative Research Center TRR142 (Project B01).

APPENDIX A: BAND STRUCTURE EFFECTS

In the main part we limited our calculation to the Zeeman effect [Eq. (16)] in the basis of $\{\Gamma_2^+, \Gamma_{5yz}^+, \Gamma_{5zx}^+, \Gamma_{5xy}^+\}$. Here we add band structure effects to the diagonalization of the Hamiltonian. We take the sum of the **B**-dependent Zeeman matrix as given in Ref. [22] and the **k**-dependent band structure matrices as given in Ref. [14]:

$$
\begin{aligned}
&M_{\text{total}}(\Delta_3, \Delta_5, \mathbf{k}, a, b, \mathbf{B}) \\
&\quad = J_3(\Delta_3, \mathbf{k}) + J_5(\Delta_5, \mathbf{k}) + M_B(a, b, \mathbf{B}) \\
&\quad = \Delta_3 \begin{pmatrix} 0 & 0 & 0 & 0 \\ 0 & 3k_x^2 - \mathbf{k}^2 & 0 & 0 \\ 0 & 0 & 3k_y^2 - \mathbf{k}^2 & 0 \\ 0 & 0 & 0 & 3k_z^2 - \mathbf{k}^2 \end{pmatrix} \\
&\qquad + \Delta_5 \begin{pmatrix} 0 & 0 & 0 & 0 \\ 0 & 0 & k_x k_y & k_x k_z \\ 0 & k_x k_y & 0 & k_y k_z \\ 0 & k_x k_z & k_y k_z & 0 \end{pmatrix} \\
&\qquad + \begin{pmatrix} \varepsilon & iaB_x & iaB_y & iaB_z \\ -iaB_x & 0 & -ibB_z & ibB_y \\ -iaB_y & ibB_z & 0 & -ibB_x \\ -iaB_z & -ibB_y & ibB_x & 0 \end{pmatrix}. \qquad \text{(A1)}
\end{aligned}
$$

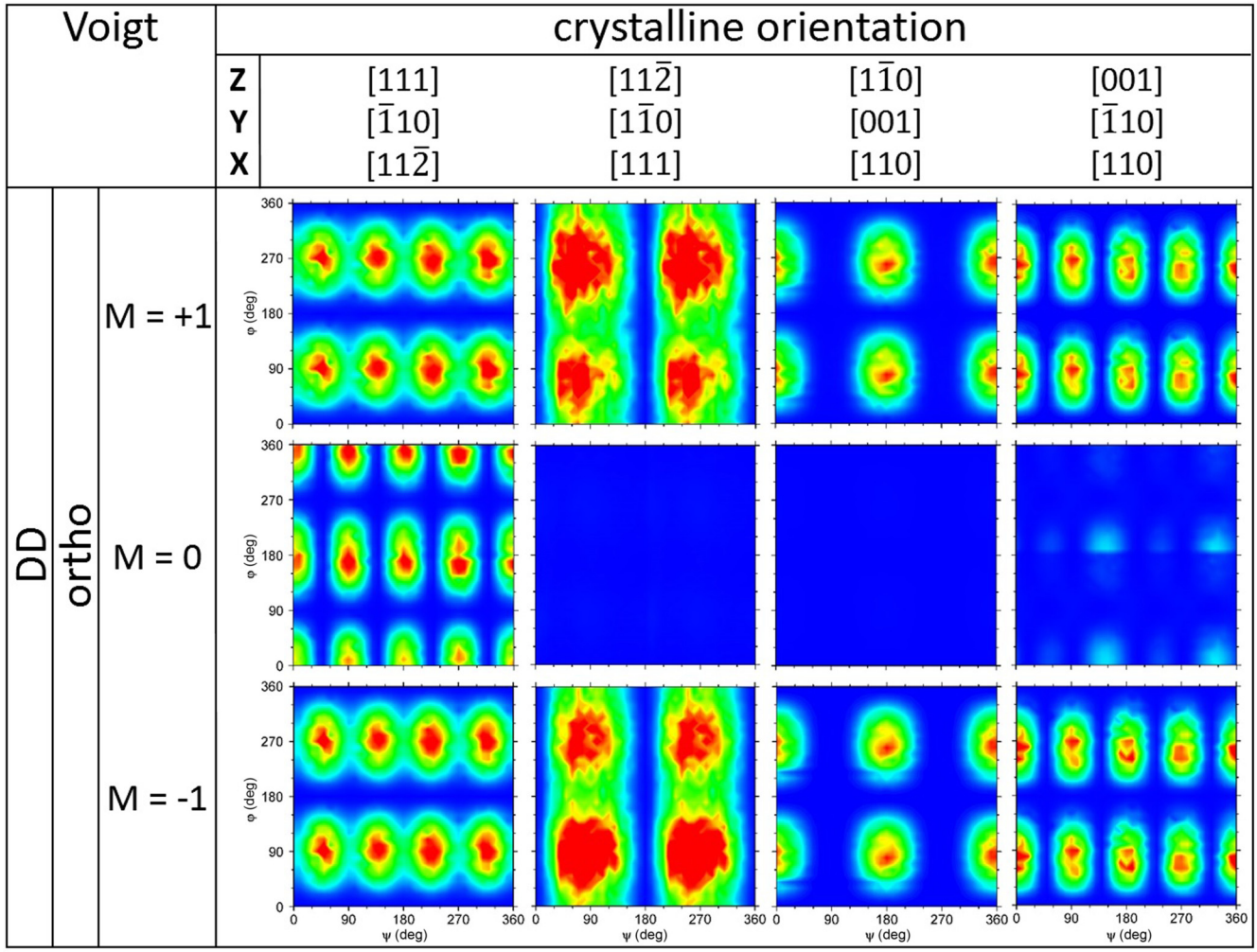

FIG. 13. Experimental data of 2D polarization diagrams of SHG of the three 1S orthoexciton components in Voigt configuration (**k** ∥ **Z** and **B** ∥ **X**) at $B = 10$ T for four selected crystalline orientations. The experimental results agree with the simulations shown in Fig. 11. A 2D diagram for the paraexciton was only measured for **k** ∥ [111] and **B** ∥ [1$\bar{1}$0] (Fig. 8). As expected, in all orientations considered, the 2D paraexciton diagrams exhibit the same polarization dependence as the $M = 0$ orthoexciton.

k is the wave vector, k_i are its components, **B** is the magnetic field, B_i are its components, $\Delta_3 = -1.3\,\mu$eV and $\Delta_5 = 2.0\,\mu$eV are the coefficients of the band structure matrices as given in Ref. [18], a corresponds to $a = \mu_B(g_c - g_v)/2$ of the main part of this paper, and b corresponds to $b = \mu_B(g_c + g_v)/2$. The resulting magnetic field dependent energies of the orthoexciton components are presented in Fig. 10.

It would be interesting to do high resolution experiments of the orthoexciton components in the low-field regime ($0 \leqslant B \leqslant 0.5$ T), where M is not a good quantum number due to mixing by the $\mathbf{k}^2$ terms in Eq. (A1). For the low-symmetry orientation **k** ∥ [112] there is a splitting into three components expected [18]. From the magnetic-field dependent eigenvectors one can derive how the three components at $B = 0$ can be characterized with increasing magnetic field by M quantum numbers (similar to the Paschen-Back effect in atomic spectroscopy).

APPENDIX B: SHG POLARIZATION DIAGRAMS FOR DIFFERENT CRYSTAL ORIENTATIONS

In this paper we have presented theoretical and experimental 2D polarization diagrams for selected orientations. In Faraday configuration SHG experiments with linearly polarized light have to take Faraday rotation in the sample as well as in the windows of the cryostat into account. In Faraday configuration measurements with circularly polarized light are therefore more appropriate. SHG with circularly polarized light for arbitrary crystalline orientation was addressed in Ref. [28]. Our derivation applies to any crystalline and magnetic field orientation. In the following, we extend the derivation for the four components to other crystalline orientations and present for each orientation 2D polarization diagrams for two selected magnetic field orientations (Voigt configuration in Fig. 11 and Faraday configuration in Fig. 12). Additional experimental data for Voigt configuration are shown in Fig. 13 and can be compared to the corresponding diagrams in Fig. 11.

[1] D. W. Snoke and G. M. Kavoulakis, Bose-Einstein condensation of excitons in Cu_2O: progress over 30 years, Rep. Prog. Phys. **77**, 116501 (2014).

[2] J. Brandt, D. Fröhlich, Ch. Sandfort, M. Bayer, H. Stolz, and N. Naka, Ultranarrow Optical Absorption And Two-Phonon Excitation Spectroscopy Of Cu_2O Paraexcitons In A High Magnetic Field, Phys. Rev. Lett. **99**, 217403 (2007).

[3] G. M. Kavoulakis, Y.-C. Chang, and G. Baym, Fine structure of excitons in Cu_2O, Phys. Rev. B **55**, 7593 (1997).

[4] A. Mysyrowicz, D. P. Trauernicht, J. P. Wolfe, and H.-R. Trebin, Stress dependence of the paraexciton in Cu_2O, Phys. Rev. B **27**, 2562 (1983).

[5] G. Kuwabara, M. Tanaka, and H. Fukutani, Optical absorption due to paraexciton of Cu_2O, Solid State Commun. **21**, 599 (1977).

[6] D. Fröhlich and R. Kenklies, Polarization dependence of two-photon magnetoabsorption of the 1*S* exciton in Cu_2O, Phys. Stat. Sol. (b) **111**, 247 (1982).

[7] Y. Liu and D. Snoke, Resonant two-photon excitation of 1*s* paraexcitons in cuprous oxide, Solid State Commun. **134**, 159 (2005).

[8] Ch. Sandfort, J. Brandt, Ch. Finke, D. Fröhlich, M. Bayer, H. Stolz, and N. Naka, Paraexcitons of Cu_2O confined by a strain trap and high magnetic fields, Phys. Rev. B **84**, 165215 (2011).

[9] N. Naka and N. Nagasawa, Nonlinear paraexciton kinetics in a potential trap in Cu_2O under two-photon resonance excitation, Phys. Rev. B **65**, 245203 (2002).

[10] D. Fröhlich, M. Itoh, and Ch. Pahlke-Lerch, Two-Photon Spectroscopy Of Odd-Parity States, Phys. Rev. Lett. **72**, 1001 (1994).

[11] J. S. Michaelis, K. Unterrainer, E. Gornik, and E. Bauser, Electric and magnetic dipole two-photon absorption in semiconductors, Phys. Rev. B **54**, 7917 (1996).

[12] A. Farenbruch, J. Mund, D. Fröhlich, D. R. Yakovlev, M. Bayer, M. A. Semina, and M. M. Glazov, Magneto-Stark and Zeeman effect as origin of second harmonic generation of excitons in Cu_2O, Phys. Rev. B **101**, 115201 (2020).

[13] G. F. Koster, J. O. Dimmock, R. G. Wheeler, and H. Statz, *Properties of the Thirty-Two Point Groups* (M. I. T. Press, Cambridge, MA, 1963).

[14] F. Schweiner, J. Main, M. Feldmaier, G. Wunner, and C. Uihlein, Impact of the valence band structure of Cu_2O on excitonic spectra, Phys. Rev. B **93**, 195203 (2016).

[15] Y. R. Shen, *The Principles of Nonlinear Optics* (Wiley, New York, 1984).

[16] D. Fröhlich, A. Kulik, B. Uebbing, A. Mysyrowicz, V. Langer, H. Stolz, and W. von der Osten, Coherent Propagation And Quantum Beats Of Quadrupole Polaritons In Cu_2O, Phys. Rev. Lett. **67**, 2343 (1991).

[17] J. Brandt, D. Fröhlich, Ch. Sandfort, M. Bayer, and H. Stolz, Paraexciton polariton propagation beats in cuprous oxide, Phys. Status Solidi C **6**, 556 (2009).

[18] G. Dasbach, D. Fröhlich, R. Klieber, D. Suter, M. Bayer, and H. Stolz, Wave-vector-dependent exchange interaction and its relevance for the effective exciton mass in Cu_2O, Phys. Rev. B **70**, 045206 (2004).

[19] J. Mund, Ch. Uihlein, D. Fröhlich, D. R. Yakovlev, and M. Bayer, Second harmonic generation on the yellow 1*S* exciton in Cu_2O in symmetry-forbidden geometries, Phys. Rev. B **99**, 195204 (2019).

[20] G. Baldassarri H. von Högersthal, G. Dasbach, D. Fröhlich, M. Kulka, H. Stolz, and M. Bayer, Dynamic band gap shifts and magneto-absorption of Cu_2O, J. Lumin. **112**, 25 (2005)

[21] M. Certier, J. B. Grun, and S. Nikitine, Etude de l'effet Zeeman de la raie n = 1 de la série jaune de Cu_2O à 20° K, J. Phys. France **25**, 361 (1964)

[22] G. Baldassarri Höger von Högersthal, D. Fröhlich, M. Kulka, Th. Auer, and M. Bayer, Acoustic and optical phonon scattering of the 1*S* yellow orthoexciton in Cu_2O, Phys. Rev. B **73**, 035202 (2006).

[23] M. Inoue and Y. Toyozawa, Two-photon absorption and energy band structure, J. Phys. Soc. Jpn. **20**, 363 (1965).

[24] G. Battaglia and G. Vetri, Dynamic Zeeman effect in paramagnetic emission and second harmonic generation, J. Phys. C: Solid State Phys. **15**, 251 (1982).

[25] M. Guccione, M. Li Vigni, and G. Vetri, The dynamic Zeeman effect in the two-photon resonance condition, J. Phys. C: Solid State Phys. **19**, 1813 (1986).

[26] D. Fröhlich, A. Nöthe, and K. Reimann, Observation Of The Resonant Optical Stark Effect In A Semiconductor, Phys. Rev. Lett. **55**, 1335 (1985).

[27] D. Fröhlich and M. Bayer, Emission of Cu_2O paraexcitons confined by a strain trap: Hints of a Bose-Einstein Condensate? Phys. Sol. State **60**, 1600 (2018).

[28] J. Mund, D. Fröhlich, D. R. Yakovlev, and M. Bayer, High-resolution second harmonic generation spectroscopy with femtosecond laser pulses on excitons in Cu_2O, Phys. Rev. B **98**, 085203 (2018).